ELSEVIER

Journal of Nuclear Materials 303 (2002) 115–124

journal of nuclear materials

www.elsevier.com/locate/jnucmat

Determination of the helium diffusion coefficient in nuclear waste storage ceramics by a nuclear reaction analysis method

Dominique Gosset [a,*], Patrick Trocellier [b], Yves Serruys [c]

[a] CEA Saclay, DMN/SRMA/LMS, F-91191 Gif/Yvette, France
[b] CEA Saclay, DSM/DRECAM/LPS, F-91191 Gif/Yvette, France
[c] CEA Saclay, DMN/SRMP, F-91191 Gif/Yvette, France

Received 6 November 2001; accepted 18 March 2002

Abstract

Host matrices for actinide immobilisation will undergo the formation of large helium quantities due to alpha decay. Helium diffusion rate has to be known in order to predict the long-term behaviour of the material, and particularly, the influence of helium accumulation on mechanical properties. A nuclear reaction analysis method, namely the $^3He(d, p)^4He$ reaction, has been used to analyse the evolution of ^3He profiles after ion implantations at 1 and 3 MeV in two materials, monoclinic ZrO_2 (as a test material) and $Ca_9Nd(PO_4)_5(SiO_4)F_{1.5}(OH)_{0.5}$ britholite (envisaged for Am and Pu long-term storage). Two data processing methods are used: the classical excitation curve (proton yields versus deuteron energy) and second, the proton energy spectrum for a given deuteron energy. The characteristics of the ^3He profiles (depth, width) obtained by both methods are compared to SRIM estimations. Their evolution during subsequent annealings allows an estimation of the helium diffusion rate in the britholite: $D\ (cm^2/s) = (2.5 \pm 1.5) \times 10^{-4} \exp(-(1.07 \pm 0.03\ eV)/kT)$ in the temperature range 200–400 °C, in agreement with previous results on similar materials. Moreover, the shape of the proton energy spectra suggests channeling effects in britholite.

1. Introduction

To incorporate minor actinides (Np, Pu, Am, Cm), in the frame of long-term storage of nuclear wastes, new materials, with compositions partially based on natural analogues are considered [1,2]. Among these, apatites are considered for Pu and Am storage. Radioactive decay of these elements leads to the formation of 7–8 helium atoms per actinide atom on the average, each with an energy release ranging from 4 to 9 MeV. Hence, the design of the storage site requires the knowledge of the helium diffusion rate in the matrix in a large temperature range. Geological studies, aiming at mineral dating by nuclear methods (e.g. U/Th/He), have led to upper limits (see e.g. [3,4] for natural apatites), but few data are available to allow a precise estimation of this diffusion rate [5] at the beginning of the life of the repository site.

In order to obtain an estimation of the diffusion coefficient, we have used the $^3He(d, p)^4He$ reaction. A three-step procedure is used [6]. First, ^3He implantations were performed to simulate radiogenic helium. Second, $^3He(d, p)^4He$ reaction was used to determine the characteristics of the implanted helium peak, mainly mean depth and width. At last, an Arrhenius plot was made from the evolution of the width of the helium profiles after annealing. This analytical method has several advantages: high selectivity (no other reactions induced by deuterons in the proton energy range of interest), probing of the material at depths large enough to avoid surface distortion effects and good sensitivity to the

* Corresponding author.
E-mail addresses: dgosset@cea.fr (D. Gosset), trocellier@drecam.cea.fr (P. Trocellier), yves.serruys@cea.fr (Y. Serruys).

0022-3115/02/$ - see front matter
PII: S0022-3115(02)00822-X

shape of the helium profile. Two variants of this nuclear reaction analysis (NRA) method are used [7]: the first approach is to map the yield of the reaction products as a function of the incident particle energy (excitation curve method, Section 3.1), the alternative approach is to make use of the energy distributions of the emitted particles for a given incident particle energy (Section 3.2).

In this paper, preliminary results are presented, mainly focussing on the data processing methods developed to analyse the helium profile characteristics.

2. Experimental

2.1. Materials

The zirconia samples have been elaborated from a high purity (99.95%) fine grain (<20 μm) powder. High density pellets were obtained by uniaxial hot pressing for 15 min at 1850 °C, 30 MPa in a graphite die under vacuum. To limit chemical reaction, a 100 μm thick tantalum foil was introduced between the die, the pistons and the powder. A pyrolitic graphite foil (Papyex®) introduced between the die and the tantalum foil facilitates sliding during densification. Zirconia undergoes a monoclinic/quadratic transition around 1000 °C characterised by large cell volume variations and distortions. To avoid subsequent cracking of the pellets during cooling, the pressure was maintained down to 600 °C, allowing plastic deformation down to relatively low temperatures. High density (5.5 g/cm^3, >95%), fine (<40 μm), homogeneous grain size, purely monoclinic (quadratic phase under limit of detection by X-ray diffraction analysis) and crack-free pellets are then obtained. They are subsequently machined (discs 1 mm thick, 12 mm diameter), annealed (800 °C under air) to restore the ZrO_2 stoichiometry and finally polished for subsequent analysis.

The britholite (fluoroapatite) samples have been obtained by calcination of the precursors in a platinum crucible and grinding. Neodymium was added as a Pu simulating material. The powder is then hot pressed in a graphite die, with a boron nitride diffusion barrier. The pellets have a high density (3.45 g/cm^3, i.e. >95%) and a heterogeneous microstructure, made of two populations of clusters (100–500 μm large) with very different grain sizes (around 5 and 50 μm). The composition has been obtained by WDS-EPMA analysis (Table 1). Setting Ca + Nd = 10 leads to the formula $Ca_{8.97}Nd_{1.03}(PO_4)_{4.83}(SiO_4)_{0.92}F_{1.6}(OH)_{0.4}$. Following [8], the fluorine deficit has been compensated by introducing (OH) groups. The crystal structure is in agreement with [8] (hexagonal cell, $a = 0.94004(37)$ nm and $c = 0.69040(29)$ nm). The pellets have been machined into 2 mm thick, 10 mm diameter discs, which were then polished.

Table 1
Composition of the britholite samples, as deduced from WDS analysis

Element	WDS
Si	0.0221
P	0.1156
Ca	0.2147
Nd	0.0246
O	0.5846
F	0.0384
Ca/Nd	8.73
P/Si	5.24

Oxygen is obtained from the individual oxide formulae.

2.2. ^{3}He implantations

^{3}He ion implantations have been performed at two different energies:

(1) 1 MeV implantations have been performed at CEA/DEN/Sac/DMN/SRMP. The sample holder was cooled using liquid nitrogen, ensuring a sample temperature well below 200 K during the implantations. The flux was homogeneous on the whole implanted surface (disc diameter 20 mm, min/max difference <10%). The doses are around 10^{16} cm^{-2}, i.e. around 10^{20} cm^{-3} at the peak maximum. For sensitivity tests, a zirconia sample has been doubly implanted at 0.3 and 1.0 MeV.
(2) 3 MeV implantations were performed at the PHASE laboratory (CNRS, Strasbourg). The sample holder was at room temperature and, due to bad fixing, the temperature of the sample could be as high as 200 °C during the implantation. The flux is heterogeneous (a factor of 2–5 from the centre to the periphery of the samples has been observed). The maximum doses are 1.5×10^{16} cm^{-2}, leading to the maximum ^{3}He concentration of around 10^{20} cm^{-3}.

The characteristics of the implanted peaks have been estimated with SRIM [9] from the stoichiometric formula and theoretical densities of the materials (given the expected ^{3}He ranges and grain sizes, no porosity has to be taken into account) as given in Table 2. For further analysis, the calculated profiles have been fitted with the gaussian function: the latter have characteristics (depth and width) somewhat different from SRIMs estimations of ranges and stragglings, due to the lower weight attributed to the low depth tail of the distributions.

2.3. Nuclear microprobe

The ^{3}He(d, p)^{4}He NRA measurements have been performed using the nuclear microprobe facility of the

Table 2
SRIM estimations and gaussian curve fitting of the characteristics of the ^{3}He peaks in zirconia and britholite

Numbers in μm	SRIM		Gauss curves		
	Range	Straggling	Mean depth	σ	FWHM
Zirconia, $d = 5.8$ g/cm^3					
0.3 MeV	0.751	0.115	0.786	0.082	0.193
1 MeV	1.92	0.153	1.99	0.091	0.214
3 MeV	6.98	0.248	7.06	0.139	2.355
Britholite, $d = 3.45$ g/cm^3					
1 MeV	2.61	0.150	2.70	0.114	0.269
3 MeV	9.12	0.220	9.22	0.158	0.372

'Laboratoire Pierre Süe' in Saclay (CEA-DSM/DRECAM and CNRS). This facility is described elsewhere [10]. Schematically, it is based on a 3.75 MV single ended Van de Graaff accelerator equipped with two microbeam lines. This machine is able to supply proton, deuteron, helium-3 or helium-4 ion beams in the energy range from 400 keV to 3.75 MeV. An object-slit system and a focusing quadrupole device permit to obtain 1×1 to 100×100 μm^2 beam spots.

The vacuum chamber is operating between 5×10^{-7} and 10^{-6} Torr. It contains a vertical sample holder (6 positions) controlled by step motors allowing 4 degrees of freedom (3 translations and 1 tilt), an optical microscope and 4 detectors: a Si–Li X-ray detector to register yields from particle induced X-ray emission (PIXE) and 3 surface barrier detectors to record scattered ions, recoiled ions and nuclear reaction products.

In order to detect the 12–14 MeV protons from the nuclear reaction induced by deuterons on helium-3, a 1500 μm thick annular surface barrier sandwich consisting of three 500 μm thick annular silicon slices has been used. Some connection problems were encountered during spectrum recording and a satellite proton peak has appeared approximately 3.5 MeV below the total energy peak. Its intensity is approximately 30% of the main peak. It looks like a secondary detection phenomenon with only a 1000 μm silicon detector (2 slices over 3) so that the NRA total yield was systematically corrected.

The incident deuteron energy has been made to vary in a decreasing way from 1.8 or 2.1 MeV to 750 keV. The typical beam conditions were: beam spot $\approx 50 \times 50$ μm^2, current intensity ≈ 4 nA, acquisition time ≈ 1200–2400 s. An absorber foil (9–25 μm Mylar or 32 μm aluminium foil) was placed in front of the annular detector in order to stop the backscattered deuterons. More details on the ^{3}He(d, p)^{4}He NRA measurements can be found in the review of Paszti [11] or in the paper of Lennard [7].

3. Data processing

3.1. Excitation curve method

Given a monoenergetic deuterons beam (initial energy E_d) interacting with the implanted ^{3}He, the total number of detected protons is derived from

$$N_p(E_d) = N_d(E_d)\Omega \int_{x=0}^{\infty} \frac{d\sigma(E_d(x))}{d\Omega}\rho(x)\,dx \quad (1)$$

with x being distance from the surface of the material; $\rho(x)$, helium-3 concentration at depth x; $d\sigma/d\Omega$, differential cross-section of the ^{3}He(d, p)^{4}He reaction calculated in the actual experimental configuration for a deuteron energy $E_d(x)$, with

$$E_d(x) = E_d - g(x),$$

actual energy of the interacting deuterons at depth x;

$$g(x) = \int_0^x \frac{\partial E_d}{\partial u}\,du,$$

deuteron energy loss from the sample surface to the depth x;

$$\frac{\partial E_d}{\partial u}(= S(E_d)),$$

stopping power of the deuterons in the material; N_d being number of deuterons of initial energy E_d; Ω, solid angle of the proton detector.

From the analysis of the $N_p(E_d)$ curve obtained for different deuteron energies, it is theoretically possible to obtain the profile $\rho(x)$ as long as this profile is not too complex. This is the classical excitation curve method. It requires a good knowledge of the stopping power of the incident deuterons in the material and of the (d, p) reaction cross-section. The stopping power of the deuterons has been estimated with SRIM. To allow the numerical integration of Eq. (1), we have used polynomial fittings as shown in Fig. 1 (residual deviation $<1\%$), which allows more straightforward calculations than more sophisticated interpolation methods. Several estimations of the (d, p) reaction differential cross-section are available (see for example [12] or [13,14] for recent reviews in the frame of fusion research). They show some differences but no available experiment allows a valuable choice. The more recent evaluations, proposed as polynomial or spline functions and partially based on theoretical considerations, are however claimed to be more trustable. To take into account the take-off angle of the proton detector (around 175° instead of 86° in [12]), a kinematic correction has to be performed (Fig. 2):

$$\sigma(\theta, E_d) = \sigma_{CM}(E_d)\frac{K}{\sqrt{AC}\sqrt{D/B - \sin^2\theta}} \quad (2)$$

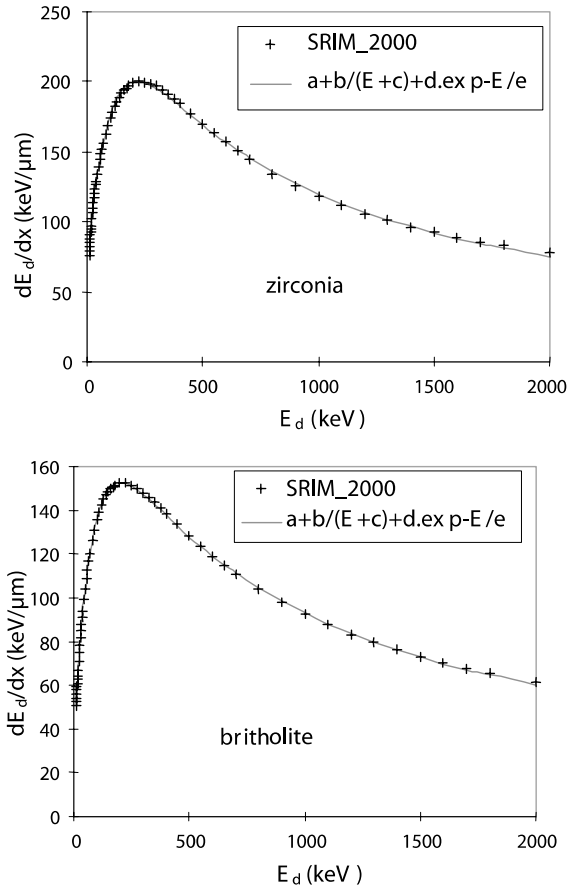

Fig. 1. Deuteron stopping power in zirconia and britholite, as calculated from SRIM (+) and fitting (—).

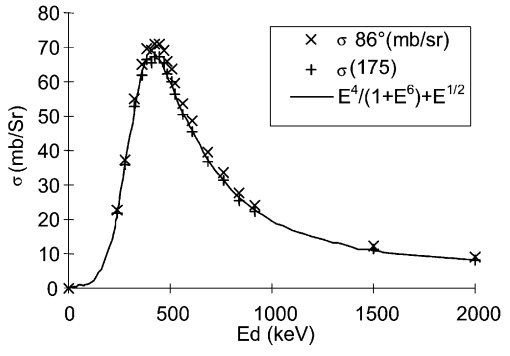

Fig. 2. (d, p) reaction differential cross-section, from [9] (×), with kinematic correction for a detector angle = 175° (+), and fitting (—).

with $\sigma_{CM}(E_d)$ being (d, p) reaction cross-section in the center of mass frame; θ, mean angle of the proton detector with respect to the incident deuteron beam = 175°;

$$K = B[\cos\theta + (D/B - \sin^2)^{1/2}]^2,$$

$$A = A'E_0/E_t, \qquad A' = M_1M_4/\text{Det.},$$

$$B = B'E_0/E_t, \qquad B' = M_1M_3/\text{Det.},$$

$$C = C'(1 + (M_1Q)/(M_2E_t)), \qquad C' = M_2M_3/\text{Det.},$$

$$D = D'(1 + (M_1Q)/(M_2E_t)), \qquad D' = M_2M_4/\text{Det.},$$

Det. $= (M_1 + M_2)(M_3 + M_4)$; M_1 being atomic mass of incident deuteron; M_2, atomic mass of helium 3; M_3, atomic mass of proton; M_4, atomic mass of helium 4; E_0, energy of incident deuteron; Q, energy of the (d, p) reaction in the center of mass frame = 18.352 keV; $E_t = E_0 + Q$.

The excitation curve method fails in determining the characteristics of complex profiles, because Eq. (1) cannot generally be deconvoluted. It is necessary to use numerical methods and make approximations. In our case, the as-implanted ^{3}He profiles, as suggested by SRIM simulations, are assumed to be gaussian (except for the low-depth tail). On the other hand, an estimation of the helium diffusion coefficient can easily be obtained provided the profile can be described by a gaussian curve (4.2.2). We then assume here that the helium profiles for both as-implanted and annealed samples, can be described with such a gaussian form:

$$\rho(x) = \frac{c_{He}}{\sigma_{He}\sqrt{2\pi}} \exp\left(-\frac{(x - x_m)^2}{2\sigma_{He}^2}\right) \tag{3}$$

with c_{He} being total ^{3}He surfacic density; σ_{He}, variance (full width at half-maximum FWHM $= \sigma_{He}\sqrt{8\ln(2)}$); x_m, mean depth of the profile.

The only parameters to be determined are c_{He}, σ_{He} and x_m, here using a numerical method (minimisation of residual deviation by dichotomy). Good accuracy is obtained for $N_p(E_d)$ data with at least 10 points. Numerical simulations of excitation curves for expected cases are presented on Fig. 3(a).

3.2. Energy spectrum analysis

The excitation curve method, however, has major limitations. First, recording the $N_p(E_d)$ curve requires long-duration experiments. Next, its main drawback is that it can only lead to a coarse description of the actual helium profile. Coming back to Eq. (1), the energy spectrum of the detected protons for a given deuteron energy is only a convolution of the ^{3}He depth profile by the (d, p) reaction cross-section:

$$\frac{dN_p}{dE_p}(E_p) = N_d(E_d)\Omega \frac{d\sigma(E_d - g(x))}{d\Omega}\rho(x)\,dx. \tag{4}$$

This is then much more sensitive to the actual ^{3}He depth profile than the excitation curve and provides a better

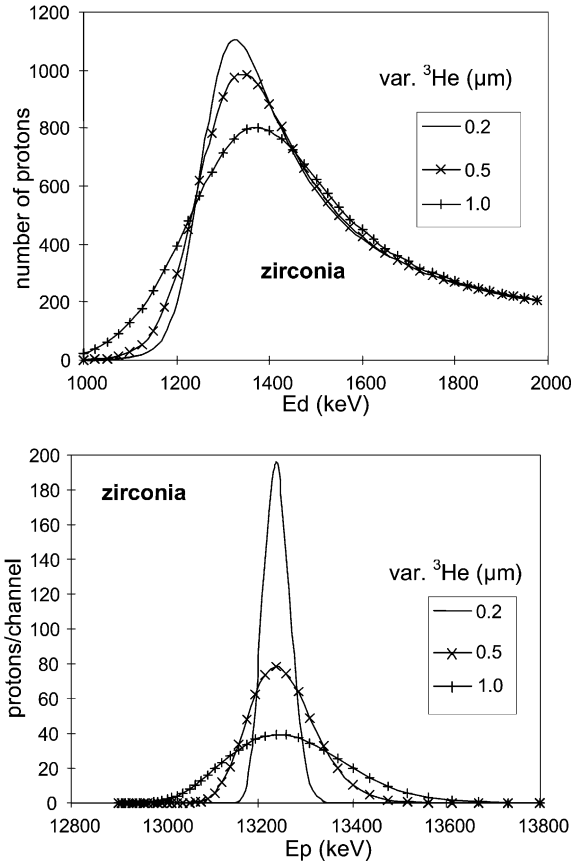

Fig. 3. Simulation of the results of a nuclear microprobe experiment (zirconia sample, max. $^3He = 10^{20}$ cm^{-3}, gaussian profile, depth = 7 μm, deuteron doses = 10 μC) for ^{3}He profile variances = 0.2, 0.5 and 1.0 μm: (a) excitation curves (deuteron energy ranging from 1000 to 2000 keV); (b) proton energy spectra (deuteron energy = 1400 keV), without stragglings.

depth resolution. In order to obtain a proton energy spectrum matching as well as possible the helium profile, the cross-section should be relatively flat in the energy range where the interactions occur, i.e. on the high energy side of the $d\sigma/d\Omega(E_d)$ curve (Fig. 2). This determines the suitable deuteron energy range. Owing to the broad resonance of the $\sigma(E_d)$ (or equivalently $\sigma(x)$) curve, this requirement is obtained in the case of narrow profiles (see e.g. Section 4.1, ZrO_2 implanted with 0.3 and 1.0 MeV ^{3}He) but also for the broader profiles obtained after 3 MeV implantations and subsequent annealings. In that case, the deuteron energy has to be at least around 1400 keV.

As compared to the excitation curve method, further parameters have to be taken into account:

- channel-energy calibration of the proton detector: this will be discussed below;
- energy of the detected proton: initial energy, energy losses in the sample and the absorber foil.

With the same notations as in Eq. (2), the energy of the emitted proton in the laboratory frame is given by

$$E_p = E_t B[\cos\theta + (D/B - \sin^2\theta)^{1/2}]^2. \quad (5)$$

The energy loss of the protons through the sample and the absorber (Al or Mylar) has been calculated with SRIM. Since only the high energy part of the curves is to be used ($E_p \approx 13$ MeV), hyperbolic approximations have been used in the following. A simulation of the proton energy distributions is reported in Fig. 3(b).

3.3. Stragglings

In both methods, the main limitation in the helium profile description comes from the energy stragglings of the incident deuterons and emitted protons in the materials. From [15], an approximation of the straggling for intermediate energy losses ($0.01 < \Delta E/E < 0.2$), is given by Bohr's formula:

$$\Sigma_B = 0.395z\left(\frac{Z}{A}d\right)^{1/2} \quad (6)$$

with Σ being variance in MeV of the energy distribution of the particles, similar to a Gauss curve; E_0, incident particle energy (MeV); m, z, atomic mass and number of the incident particles; A, Z, atomic mass and number of the target (in the case of polyatomic targets, average values weighted by the atomic fractions); x, particle range (cm); d, target density (g/cm^3).

For high energy losses ($0.2 < \Delta E/E < 0.8$), an estimation of the straggling can be obtained from Tschalär [15]:

$$\frac{\Sigma_T^2}{\Sigma_B^2} = \frac{S^2(\overline{E(x)})}{dx}\int_{\overline{E(x)}}^{E_0}\frac{dE}{S^3(E)}, \quad (7)$$

where $S = dE/dx$ is the stopping power and $\overline{E(x)}$ the mean energy at depth x.

The component of the total energy straggling of the protons arising from the deuteron straggling is obtained from simplification of the kinematic formula for $\theta = 180°$:

$$\frac{\partial E_p}{\partial E_d} = B' + D' - \sqrt{B'D'}\frac{2E_d + Q(1 + M_1/M_2)}{\sqrt{E_d^2 + QE_d(1 + M_1/M_2)}} \approx -1 \quad \text{for } E_d = 500 \text{ keV}. \quad (8)$$

Assuming normal distributions, the total straggling of the detected protons is then obtained by the quadratic sum of the different components (incident deuterons and emitted protons in the samples and protons in the absorber). Applying these formulae to the outcoming

protons leads to stragglings around 10–20 keV in each material (sample and absorbers). When using the proton energy curve method, this will hide details in the helium distribution smaller than approximately 0.1 μm: this is then the resolution limit of this method.

But the main straggling effect arises from the incident deuterons: in the energy range and depths of interest here (respectively $E_d = 1$–2 MeV and $x = 6$–8 μm), the Tschalär formula leads to values around 50–60 keV. For both methods, this induces an apparent broadening of the helium distributions. In the case of the materials implanted with 3 MeV ^{3}He, and assuming gaussian helium distributions, the apparent variances are increased by about 0.15–0.20 μm. This is comparable to the effective variances after implantation, as estimated by SRIM, and should then be taken into account. In the preliminary estimations we present here, we consider this effect as a systematic error, which can then be neglected, to first order, since the helium diffusion coefficients are estimated from variance differences (see Section 4.2.2).

4. Results and discussion

4.1. Monoclinic zirconia

An example of excitation curve and subsequent analysis obtained from a monoclinic zirconia sample is reported in Fig. 4. The sample has been implanted with 3 MeV ^{3}He at an expected dose of around 2×10^{16} cm^{-2}. The analysis has been performed with a 5 nA deuteron microbeam (50×50 μm^2). The deuteron dose at each energy (decreasing from 1800 to 1000 keV) is 5 μC, inducing a recording time of approximately 1000 s for each energy. In order to stop the backscattered deuterons, a 32 μm thick aluminium foil is placed in front of the proton detector; this induces a too large energy straggling to allow a relevant analysis of the proton energy spectra. The calculated curve is obtained by a numerical simulation of the experiment from Eq. (1), in which the integral is discretised with a 0.02 μm depth step and using polynomial approximations of the deuteron stopping power and the (d, p) reaction differential cross-section data. The ^{3}He profile parameters are then obtained through a classical convergence method by dichotomy, leading to the following values:

Depth of maximum ^{3}He concentration: 6.61 ± 0.02 μm;
Variance of ^{3}He distribution: 0.37 ± 0.02 μm;
i.e. FWHM: 0.87 μm;
^{3}He dose: $2.40 \pm 0.05 \times 10^{16}$ cm^{-2};
Maximum ^{3}He concentration: $2.58 \pm 0.16 \times 10^{20}$ cm^{-3}.

These values are compared to SRIM estimations (Table 2). It appears that the ^{3}He profile characteristics (depth and width) are very different: calculated depth 6% lower, twofold variance. As mentioned above, the apparent broadening of the profiles can be mainly attributed to the deuteron straggling effects.

A sample has been annealed at 800 °C for 1 h. The corresponding excitation curve shows no evolution of the helium distribution, mean depth and width. This means a high trapping efficiency of helium in this material, perhaps by formation of either vacancy-helium complexes or clusters such as bubbles.

The sensitivity of the proton energy spectrum method has been evaluated with a sample that has been implanted with 0.3 and 1.0 MeV ^{3}He. The analysis is performed with a 800 keV deuteron beam. This allows the use of a very thin absorber, here a 12.5 μm thick Mylar foil. In that case, proton straggling is drastically lowered and the resulting proton energy spectrum clearly exhibits two peaks, corresponding to the two helium layers as shown in Fig. 5. The analysis has been performed from

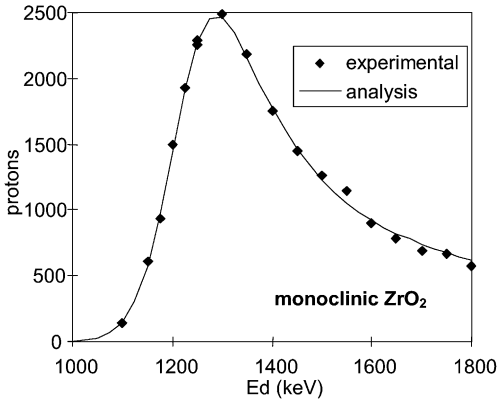

Fig. 4. Excitation curve and corresponding analysis for a zirconia sample (3 MeV ^{3}He implantation).

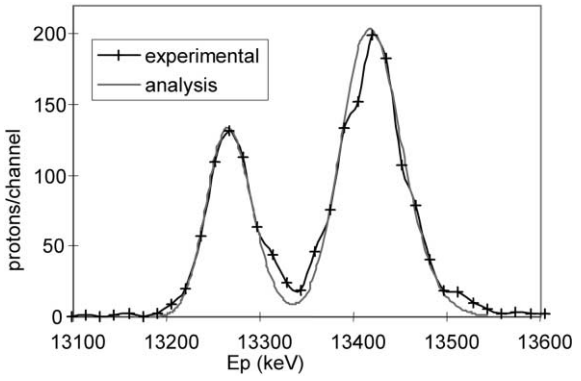

Fig. 5. Proton energy spectrum for a zirconia sample implanted with 0.3 and 1.0 MeV ^{3}He, and analysis from Eq. (4) (deuteron energy = 800 keV).

Eq. (4). As mentioned above, this method requires a calibration of the proton detector. For the low-energy part of the detected spectra ($E_p < 5$ MeV), several characteristic nuclear reactions allow an accurate calibration, mainly those induced on ^{12}C and ^{16}O. But the extrapolation to the proton energy range of interest here (around 13 MeV) is not accurate enough. A hypothesis has to be made. We have here assumed that the actual mean depth of the deepest helium layer is given by the SRIM estimations. All other parameters have then been adjusted to obtain the best agreement with the experimental curve (Fig. 5). The following results are obtained:

Peak	Mean depth (μm)		Variance (μm)		^{3}He (10^{16} cm^{-2})
	Apparent	SRIM	Apparent	SRIM	
300 keV	0.80	0.79	0.23	0.086	0.53
1 MeV	= SRIM	1.98	0.21	0.090	0.65

The apparent widths are again very different from SRIM estimations, mainly due to straggling effects, but the depth of the first layer is correctly estimated.

4.2. Britholite

4.2.1. Channeling

The analysis of britholite has been only performed on samples implanted with 3 MeV ^{3}He, in conditions similar to zirconia analysis. But, in order to reduce the proton energy straggling, a 25 μm Mylar absorber has been used. In those conditions, the proton energy spectra show puzzling features (Fig. 6): a large tail appears on the high energy side of the main peak, which can even resolve into a secondary peak for some analysed areas. Due to kinematic effects (Eq. (5)), this corresponds to protons arising from reactions with deuterons of lower energy, i.e. at greater depths. This means that in this material, helium has been partly implanted at depths larger than those estimated by SRIM, i.e. assuming a random distribution of the atoms in the structure. Such an effect was not seen in zirconia, and should be attributed to the structure of britholite. The latter is characterised by wide channels (diameter around 0.5 nm) along the *c*-axis of the hexagonal structure, containing mainly the fluorine atoms, i.e. with a low-atomic density. In such a structure, a particle coming in a direction close to the channel axis will undergo lower energy losses as compared to the general (random) case because of the lower probability of collisions with the atoms of the structure and focussing by the channel edges. Due to experimental conditions (grains size < 5 μm, deuteron beam ~ 50 × 50 μm^2), around one hundred grains are simultaneously analysed. Therefore, we have to assume that, among these, a few grains are correctly oriented to allow this channeling effect. Here, we observed that the energy of the protons coming from the deepest (channelled) ^{3}He is around 300 keV higher than the main component of the spectra (Fig. 6). A coarse simulation shows that this corresponds to stopping powers (either for ^{3}He or deuterons, since the beams are in both cases perpendicular to the surface of the sample) only 10–20% lower than in the normal (random) material; the resulting implantation depths are increased in about the same extent.

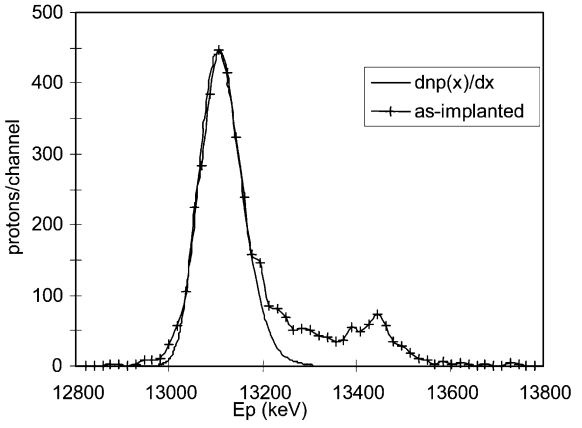

Fig. 6. Proton energy spectrum (deuteron energy = 1400 keV) for a britholite sample implanted with 3 MeV ^{3}He (+) compared with a simulation of a single gaussian ^{3}He profile (—).

It would be very interesting to analyse this effect, because of its possible consequences on helium diffusion: this could explain the hypothetical channels put forward by Soulet [2] to explain the behaviour of helium in apatite as deduced from RBS analysis. This is however beyond the scope of this paper.

4.2.2. Helium diffusion coefficient

Both data processing methods, excitation curve and proton energy spectra, have been used to estimate the helium diffusion coefficient in the britholite. For this, two samples have been implanted with 3 MeV ^{3}He. They have subsequently been cut and the different sectors annealed at different temperatures. The temperatures and durations are extrapolated from Ouchani's RBS results [5]:

T (°C)	t (h)
200	264
250	48
325	1
400	0.58

The main results are reported in Tables 3 and 4. For the as-implanted samples, the excitation curve method leads to mean depths lower than SRIM estimations (around 8.6 μm versus 9.1 μm), as in zirconia. This cannot be due to the channeling effects, which should on the opposite lead to higher depths. The widths are here again larger than SRIM estimations, but not as much as in zirconia (Table 2). On the other hand, the results show a very heterogeneous ^{3}He implantation (very different helium concentrations on the different sectors of a given sample): Fig. 7.

In the case of proton energy spectra, the channel/energy calibration of the proton detector has been built assuming a mean depth for the helium profile in the as-implanted samples given by the excitation curve method. The same calibration has then been used for analysing the spectra obtained with the annealed samples.

In both methods, the helium concentration has been assumed to have a gaussian profile. In that case, it is possible to deduce a diffusion coefficient from the variation of the variance of the distribution after the annealing steps. From [16], we have

$$\sigma_t^2 = \sigma_0^2 + 2Dt, \tag{9}$$

where σ_t being variance after annealing; σ_0, variance before annealing; t, annealing duration.

The helium diffusion coefficient can be deduced from Tables 3 and 4. Since the experiments have been performed with ^{3}He but radiogenic helium is ^{4}He, a mass correction has been performed: $D(^4\mathrm{He}) = D(^3\mathrm{He}) \times \sqrt{3/4}$. The results are reported on Fig. 8 and compared to the values obtained by RBS analysis [5] on an apatite. An Arrhenius plot can be made, leading to

Table 3
Main characteristics of helium profiles (3 MeV ^{3}He implantation) in annealed britholite obtained with the excitation curve method

	Run 1005			Run 2602			Run 3001			± (%)
	No annealing	200 °C	250 °C	No annealing	325 °C	400 °C	No annealing	325 °C	400 °C	
	–	(264 h)	(48 h)	–	(1 h)	(0.58 h)	–	(1 h)	(0.58 h)	
Filter	Mylar 25 μm			Al 32 μm			Al 32 μm			
Number of data	13			15			6			
Mean depth (μm)	8.622	8.650	8.666	8.631	8.525	8.781	8.638	8.581	8.576	0.2–0.3
Variance (μm)	0.211	0.429	0.481	0.291	0.544	1.101	0.247	0.538	1.141	4–6
FWHM (μm)	0.496	1.010	1.133	0.684	1.280	2.592	0.581	1.266	2.686	4–6
$c_{He}/10^{16}$ (cm^{-2})	2.52	0.53	2.55	2.86	2.06	1.96	2.89	2.08	1.94	0.7–2
c_{He} max $/10^{20}$ (cm^{-3})	3.41	0.47	1.77	3.92	1.51	0.71	4.67	1.55	0.68	5–7

Annealing temperatures are given in °C; duration is given in parentheses.

Table 4
Main characteristics of helium profiles (3 MeV ^{3}He implantation) in annealed britholite obtained with the proton energy spectra method (analysis of the main peak, channeling contributions neglected, straggling not taken into account)

T annealing (°C)	Proton detector calibration: 17.828 keV/channel			
	t (h)	Depth (μm)	He^3 10^{16} (cm^{-2})	Variance (μm)
Run 1005, E_d = 1400 keV[a]				
Non-annealed		8.622	1.75	0.45
200	264	8.65	0.40	0.60
250	48	8.65	0.95	0.65
	Proton detector calibration: 21.054 keV/channel			
Run 3001, E_d = 1400 keV[a]				
Non-annealed		8.622	2.68	0.48
325	1	8.47	2.67	0.62
400	0.58	8.47	2.25	0.87

[a] Depth: non-annealed = 8.622 μm (excitation curve).

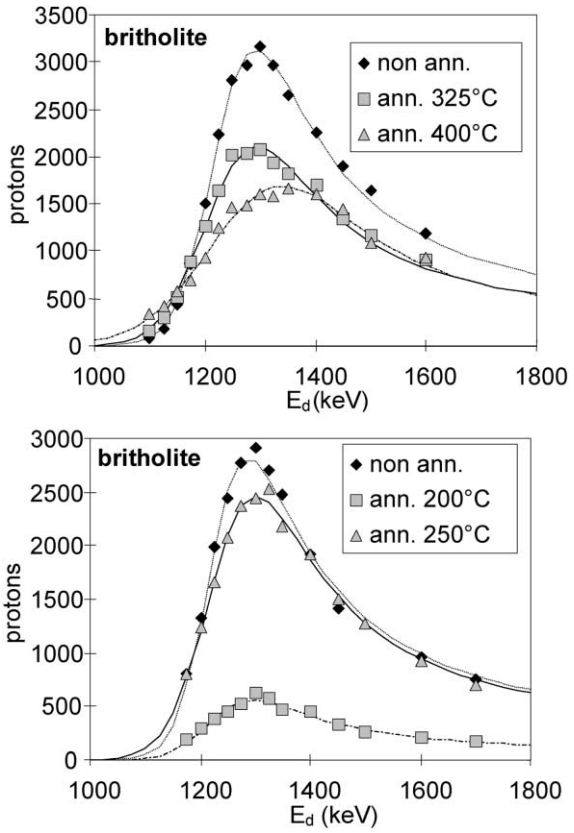

Fig. 7. Analysis of excitation curves for samples of britholite implanted with 3 MeV ^{3}He and subsequently annealed.

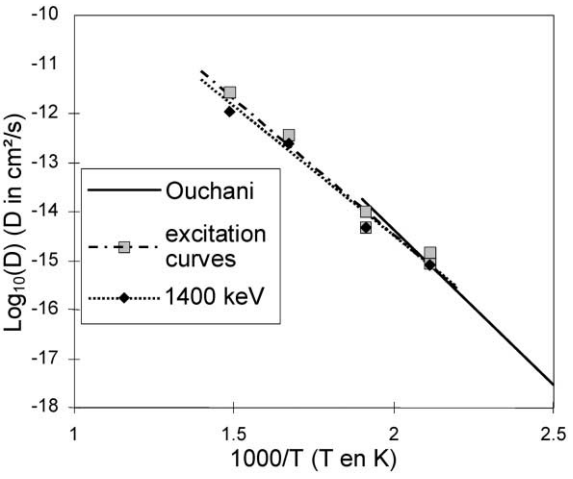

Fig. 8. Helium diffusion coefficient in britholite. Excitation curve and proton energy spectrum (deuteron energy = 1400 keV) methods, and results from [5] obtained by RBS analysis on an apatite.

the following estimations valid for T ranging from 200 to 400 °C:

$D(^4\mathrm{He}) = D_0 \exp(-E_a/\mathrm{kT})$, D in cm^2/s, E_a in eV and T in K, and
Excitation curve method: $D_0 = (4.03 \pm 0.8) \times 10^{-4}$ cm^2/s, $E_a = 1.09 \pm 0.02$ eV;
Protons energy spectra method: $D_0 = (1.89 \pm 0.7) \times 10^{-4}$cm^2/s, $E_a = 1.08 \pm 0.04$ eV.

Both methods lead to comparable results and are in agreement with Ouchani's estimations. The main approximation of the methods we use here, i.e. neglecting the stragglings, is then of low consequences in determining the diffusion coefficients.

5. Summary

In the frame of studies dedicated to the behaviour of ceramic materials considered for long-duration nuclear waste storage, we have been led to determine the diffusion coefficient of helium in these materials. For this purpose, a three-step method has been used, consisting of implanting ^{3}He, analysing the implanted profile with the ^{3}He(d, p)^{4}He reaction and deducing a diffusion coefficient from the evolution of the profile width with the annealing temperature. The analysis of helium profiles has been made according to two different methods: first, the classical excitation curve (number of collected protons for a set of deuteron energies) and second, the proton energy spectra for selected deuteron energies.

In the case of monoclinic zirconia, here used as a reference material, we have deduced mean implantation depths that are significantly smaller than SRIM estimations, which could arise from uncertainties either in stopping power or in the (d, p) reaction cross-section. The apparent width of the helium distributions is much higher than SRIM estimations, mainly due to analysis approximations (deuteron and proton stragglings are neglected). Moreover, helium is very efficiently trapped (no measurable diffusion after annealing at 800 °C).

As for britholite, the analysis of the proton energy spectra has shown a channeling mechanism in the material, possibly related to the presence of large channels in the structure. Annealing tests in the temperature range 200–400 °C have led to estimations of the helium diffusion coefficient in this material. Both methods, excitation curve and proton energy spectra, lead to comparable values, which are in good agreement with previous results on an apatite.

Further studies are needed concerning the analysis of channeling in britholite and trapping mechanisms of

helium in those materials. Improvement of data analysis, taking into account straggling effects, are in progress [17].

Acknowledgements

J.-M. Costantini (CEA Saclay, DMN/SRMA) initially proposed the (d, p) nuclear reaction method. We are very indebted in CEA/Cad/DESD/SEP/LEMC laboratory, which has elaborated the britholite samples. At last, J.J. Grob (Phase laboratory, Strasbourg) has performed the high energy implantations.

References

[1] Scientific Basis for Nuclear Waste Management XXII, MRS Symp. Proc. 556, D.J. Wronkiewicz, J.H. Lee (Eds.), Boston, MA 1998.
[2] S. Soulet, Study of self irradiation effects in apatitic materials, PhD thesis, Orsay Univ., 2001.
[3] H.J. Lippolt, L. Markus, R.S. Wernicke, B. Hagedorn, Chem. Geol. Isotope Geosc. 112 (1994) 179.
[4] P.K. Zeitler, A.L. Herczeg, I. McDougall, M. Honda, Geochem. Cosmochem. Acta 51 (1987) 2865.
[5] S. Ouchani, J.C. Dran, J. Chaumont, Appl. Geochem. 13 (6) (1998) 707.
[6] F. Zielinski, J.M. Costantini, J. Haussy, F. Durbin, Nucl. Instrum. and Meth. B, submitted.
[7] W.N. Lennard, G.R. Massoumi, P.F.A. Alkemade, I.V. Mitchell, N.S. McIntyre, R.D. Davidson, Nucl. Instrum. and Meth. B 73 (1993) 203.
[8] L. Boyer, J.M. Savariault, J. Carpena, J.L. Lacout, Acta Crystallogr. C 54 (1998) 1057.
[9] J.F. Ziegler, J.P. Biersack, www.srim.org.
[10] P.M. Trocellier, Microsc. Microanal. Microstruct. 7 (1996) 235.
[11] F. Paszti, Nucl. Instrum. and Meth. B 66 (1992) 83.
[12] J.L. Yarnell, R.H. Lovberg, W.R. Stratton, Phys. Rev. 90 (2) (1953) 292.
[13] H.S. Bosch, G.M. Hale, Nucl. Fusion 32 (4) (1992) 611.
[14] S.N. Abramovich, B.Y. Guzhovskij, V.A. Zherebtsov, A.G. Zvenigorodskij, Nuclear Physics Constants for Thermonuclear Fusion, INDC(CCP)-326/L+F (IAEA,1991).
[15] J. Tirira, Y. Serruys, P. Trocellier, Forward Recoil Spectrometry, Plenum, New York, 1996.
[16] J. Philibert, Diffusion and Matter Transport in Solids, ed. Physique, Paris, 1985.
[17] Y. Serruys, D. Gosset, P. Trocellier, work in progress.